

GPS monitoring of crustal deformation at Taal Volcano, Philippines

A.R. Lowry^{a,b,*}, M.W. Hamburger^{b,1}, C.M. Meertens^{c,2}, E.G. Ramos^d

^aGPS Science/Technology Group, University Center for Atmospheric Research (UCAR), Boulder, CO, USA

^bDepartment of Geological Sciences, Indiana University, Bloomington, IN 47405, USA

^cUNAVCO/UCAR, Boulder, CO, USA

^dPhilippine Institute of Volcanology and Seismology (PHIVOLCS), Quezon City, Philippines

Received 18 January 2000; revised 16 June 2000; accepted 16 June 2000

Abstract

Data from a dual-frequency GPS network operated continuously from May 1998–October 1999 on Taal volcano, Philippines, were processed on a daily basis to monitor processes of crustal deformation associated with volcanic activity. During the 16-month period of observations, displacements totaled nearly 30 mm in the horizontal and 50 mm in the vertical over 2.7 and 5.8 km baselines. Relative site velocities, estimated from daily site coordinates using 60-day tapered windows, vary significantly and can exceed 150 mm yr^{-1} in the horizontal. Velocity estimates were used to invert for parameters of a point-source model of elastic strain. During periods in which velocities are significant, the motions have a localized source at very high confidence, and the source magnitude term fluctuates between inflationary and deflationary behavior on time scales of weeks to months. The largest site velocities (and corresponding deformation model parameters) are time-correlative with anomalous bursts of hydrothermal activity and high-frequency local seismicity. In each instance the onset of deformation precedes both seismicity and hydrothermal activity, and the hydrothermal event coincides with a rapid shift in the velocity behavior. The relative timing of these phenomena suggests that deformation and seismicity both are responding to punctuated migration of hydrothermal fluids. © 2001 Published by Elsevier Science B.V.

Keywords: Taal; global positioning system; deformation; monitoring; volcanoes; geodesy

1. Introduction

Of the variety of methods used to evaluate volcanic hazard, crustal deformation measurements are among the most sensitive and reliable indicators of magmatic activity at depth (Banks et al., 1989; Dvorak and

Dzurisen, 1997). Terrestrial geodetic measurements such as leveling, triangulation, and trilateration have been used for nearly a century to monitor volcanic activity (e.g. Omori, 1913). Such measurements frequently show strong signals precursory to volcanic eruptions (see review in Dvorak and Dzurisen, 1997).

In recent decades, traditional surveying measurements are giving way to continuous, real-time instrumentation. Leveling and electronic distance measurements (EDM) still supplement the volcanologist's toolbox, but other instruments such as strainmeters and tiltmeters have advantages that include

* Corresponding author. Fax: +1-303-497-2610.

E-mail addresses: arlowry@ucar.edu (A.R. Lowry), eramos@phivolcs.dost.gov.ph (E.G. Ramos).

¹ Fax: +1-812-855-7899.

² Fax: +1-303-497-2610.

suitability for remote operation (hence decreasing the risk to personnel during crises) and continuous, real-time sampling of volcanic motions. New space-based techniques, including Global Positioning System (GPS) and synthetic aperture radar interferometry (InSAR), also show tremendous potential for volcano monitoring applications (Dixon et al., 1997; Wicks et al., 1998). Each of these methods provides a slightly different observable — strainmeters and tiltmeters measure various local displacement derivatives; InSAR provides change in range to a satellite; and GPS yields absolute or relative ground displacement — and each has its own particular advantages and disadvantages with regard to cost, precision, long-term stability, and temporal and spatial sampling (Silver et al., 1999). The optimal approach to understanding and monitoring volcanic processes should probably include two or more of these techniques (e.g. Dixon et al., 1997; Aoki et al., 1999).

GPS in particular yields better than one part in 10^6 accuracy over relevant distances, which is less sensitive than tiltmeters and strainmeters in the short-term but more accurate over periods exceeding a month (Silver et al., 1999). Cost for the latest generation of single-frequency instruments is comparable to that of a tiltmeter, and an order of magnitude less than for a borehole strainmeter. The decreasing cost and increasingly recognized benefits of GPS monitoring have precipitated deployment of continuous networks at several critical volcanic centers. Most results published to date describe campaign-style measurements, in which site positions were surveyed at monthly to annual intervals (e.g. Owen et al., 1995; Pingue et al., 1998; Mattioli et al., 1998; Jousset and Okada, 1999). However, volcanic processes can rapidly switch deformation behavior, and precursory strain is recognizable weeks or months prior to expressions of seismicity or surface phenomena (Langbein et al., 1993). The relatively sparse accounts of continuous network measurements focus on actively erupting basaltic volcanoes (e.g. Owen et al., 2000), where eruptive cycles are short. Recently, continuous GPS systems have also been deployed at a small number of explosive, andesitic volcanoes. In this paper, we present initial results from one of the first such continuous monitoring systems: a three-station network at Taal volcano

in the Philippines, where we find evidence for variable crustal movement associated with processes of volcanic unrest.

2. Volcano–tectonic setting

Taal volcano is one in a chain of active volcanoes associated with eastward subduction of the South China Sea (Eurasian Plate) beneath the western margin of the Philippine archipelago (Hamburger et al., 1983). The volcano is located at the intersection of the northerly-trending west Luzon calc-alkaline volcanic arc and the “Macolod Corridor”, a cross-arc lineament comprised of andesitic complex volcanoes and monogenetic basalt cones and maars (Knittel and Oles, 1995) (Fig. 1). Volcano Island, the active center of Taal volcano, is a young, ~8-km diameter volcanic edifice constructed at the center of a ~25-km diameter collapse caldera, now occupied by Taal Lake. The caldera formed following at least four major, ignimbritic eruptions between 500 and 100 ka (Listanco, 1994) and is at least partly fault-controlled, as reflected in its location at the juncture of several regional fault structures (Torres et al., 1995). Eruptive products are bimodal: Early ignimbrites are predominantly calc-alkaline dacite, whereas more recent lava flows and tephra deposits are mostly basalts and basaltic andesites with tholeiitic affinity (Listanco, 1994; Knittel and Oles, 1995).

A pair of seismic studies afford the only published constraints on subsurface geophysical structure beneath Taal. Nishigami et al. (1994) report a fan-shot seismic profile indicating increased S wave attenuation below ~1 km and strong reflectors at 7–10 km depth beneath the island. The authors interpret these seismic properties as evidence of a magma chamber between 1 and 7 km depth, but those depths are too shallow for such a widespread partial melt system to remain in stable equilibrium. More likely the velocity and attenuation anomalies correspond to hydrothermal overpressuring and alteration of volcanoclastics similar to that interpreted from seismic analyses of other large caldera systems (e.g. Miller and Smith, 1999). A ~15% reduction of shear wave velocity at 18 km depth beneath the northern caldera rim, inferred from receiver function analysis at a

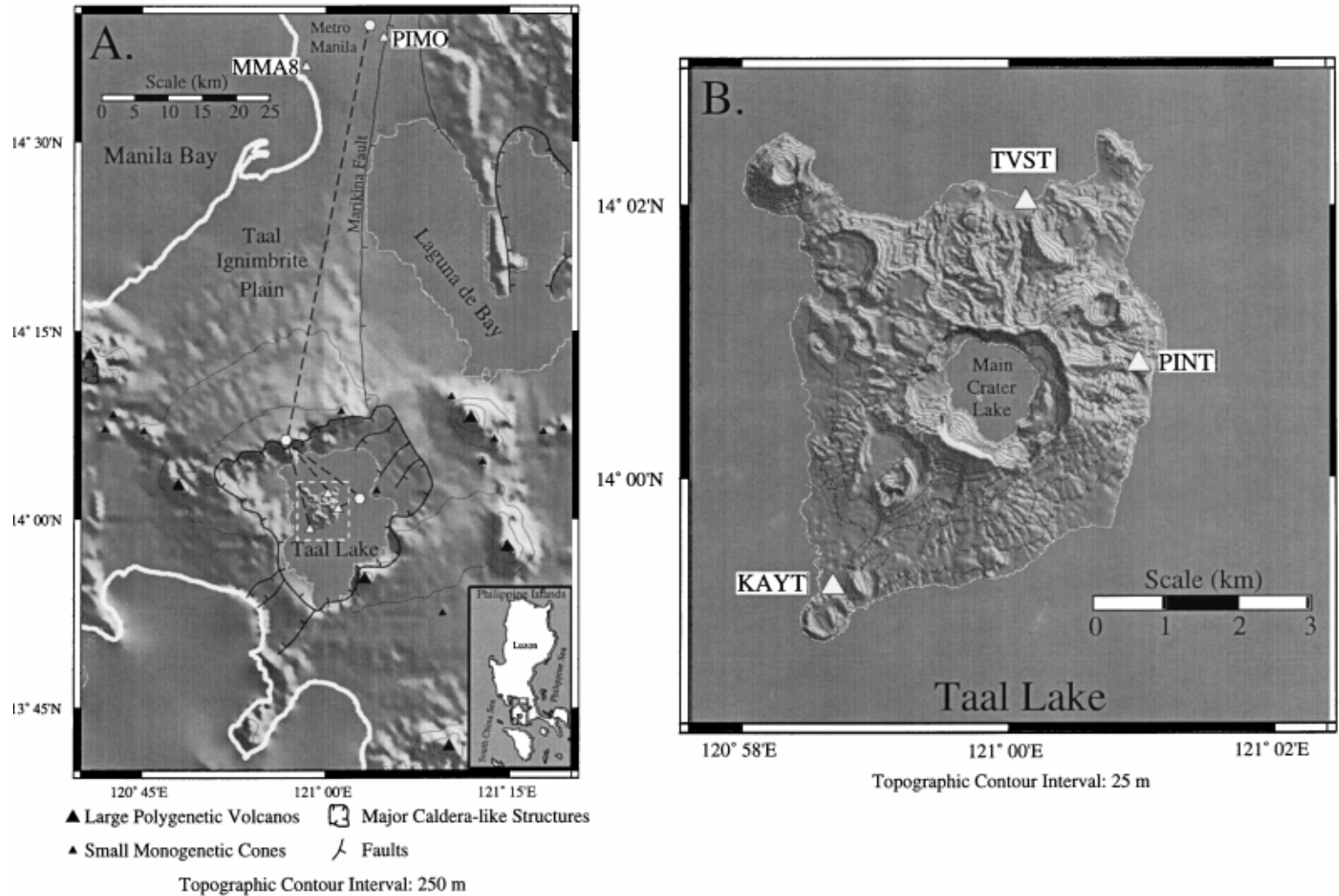


Fig. 1. Location map of Taal, superimposed on shaded relief. Dual-frequency GPS sites are indicated by white triangles; radio telemetry sites are white hexagons and communication routing paths are dotted lines. Volcanotectonic features after Torres et al. (1995). (a) Taal caldera and vicinity. Inset depicts location on island of Luzon; dashed white box is location of detail map shown in (b). (b) Taal's Volcano Island.

single seismometer, has been interpreted to indicate partial melt at that depth also (Besana et al., 1995).

There have been 33 recorded eruptions of Taal volcano in the past four centuries, including very destructive events in 1754, 1911, and 1965. Base surges, lake seiches, and toxic gas generated by the predominantly phreatic 1911 eruption took the lives of over 1300 residents of Volcano Island, and more than 200 residents died in base surges and heavy tephra airfall during the violent 1965 phreatomagmatic eruption (Moore et al., 1966). Eruptions have included phreatic and phreato-magmatic components, and have originated from both summit and flank vents (Taal Volcano Profile, 1995; Torres et al., 1995), but the eight most recent eruptions were from flanking vents along the trend of regional faults that intersect at the volcano's edifice (Fig. 1). From 1992 to the present, Taal volcano has been in an active state of unrest. Evidence of dynamism has included: (1) swarms of high-frequency volcano-tectonic earthquakes; (2) new fissures and hydrothermal activity on the flanks of Volcano Island; (3) increased temperatures in the crater lake at the volcano's summit; and (4) acoustic outgassing in the crater lake (e.g. Ramos et al., 1997).

3. Deformation monitoring networks

GPS measurement of crustal motions at Taal began in 1996 with campaign-style observation of a 15-station network surrounding the volcano. The network was reobserved in 1998 and 1999, and the 1996–1998 campaign data reveal up to 50 mm of horizontal motion directed toward the summit crater lake and as much as 80 mm of subsidence, apparently resulting from deflation following the 1992–1994 crisis (Hamburger et al., 1998; Thibault, 1999). In May of 1998, we installed a network of three continuously recording GPS stations on Volcano Island (Fig. 1). Monumentation consists of a 15-cm-diameter galvanized steel pipe cemented into lava bedrock (KAYT) or driven to refusal from a 2-m-deep excavation, then backfilled with cement (TVST and PINT). The installations include dual-frequency Trimble 4000SSE GPS receivers equipped with ground-plane antennas, powered by six 12-V batteries and three solar panels. Carrier phase and other observables are sampled at

30-s intervals, from all satellites visible above a 10° elevation mask. At the end of each UTC day, data are radio telemetered via Freewave spread-spectrum digital radio modems to the central recording site in Manila, using repeater sites on Napayun Island and atop the caldera rim (Fig. 1). Data are then transferred via ftp from the Manila recording site to UNAVCO (Boulder, Colorado) where they are archived and made available to the research community at http://www.unavco.ucar.edu/data/ftp_rinex.html. Finally the data are ftp-transferred to Indiana University for processing and analysis.

In many instances the processing and analysis (including deformation modeling) has been completed within 18–24 h after the end of UTC day. If this were achieved consistently, GPS deformation monitoring would be an effective tool for near-real-time hazard analysis. In practice the circuitous data routing has proven vulnerable to delays and interruptions at several points along the communication pathway; consequently the lag time between data collection and an updated deformation model was more typically days to weeks during the period of operation discussed in this paper. Also, the complexity of the data routing made it difficult to distinguish a typical lapse at an ftp transfer point from a more serious malfunction resulting in permanent data loss. For example, the 50-day gap in PINT data near the end of 1998 was eventually traced to a dead battery at the radio repeater station on Napayun Island. The June, 1999 gap at PINT followed relocation of that same repeater station to another site where it was visible to stations in a larger single-frequency network but no longer accessible from PINT. Subsequent PINT data were downloaded periodically by PHIVOLCS personnel on-site. Fortunately the KAYT and TVST time series are relatively complete.

4. GPS data analysis

Taal network data are processed for daily coordinates together with continuous data from two sites in Manila: (1) PIMO, instituted in November 1998 by Jet Propulsion Labs (JPL) as part of the International GPS Service for Geodynamics (IGS) network; and (2) MMA8, maintained through October 1998 by the Philippine National Mapping and Resource Information

Authority (NAMRIA) as part of the GPSWING network (Kato et al., 1998). The data are processed with Bernese version 4.0 software (Rothacher and Mervart, 1996) using a standard processing sequence that includes: (1) cycle-slip screening and outlier removal using ionosphere-free linear combination (L3) double-difference phase residuals; (2) ambiguity resolution using wide-lane (L5) and then L3 single differences; and (3) a network solution for site coordinates and tropospheric delays. Initial processing uses the IGS rapid orbit prediction combinations for precise orbit and pole information; later the data are reprocessed using IGS final orbit and pole combinations (Beutler et al., 1995) once these become available.

Because precision GPS positioning requires differencing of carrier phase, we chose to fix one site in the network (TVST) at its International Terrestrial Reference Frame (ITRF97) epoch 1998.5 position and estimate the other site coordinates in a relative sense. Coordinate error is estimated in a somewhat nonstandard fashion. The coordinate covariance matrix for the entire network solution is estimated correctly from parameter inversion statistics, transformed to local north-east-up coordinates and then the formal error is assigned as the corresponding column sum of the covariance matrix (rather than using just the main diagonal term, as is more commonly done). This results in estimates of formal error that are typically about a factor of five larger than standard estimates. Repeatability scaling factors for the error are estimated independently (one for each coordinate direction at each site) using the 95th% χ^2 repeatability of the coordinates relative to a time-varying velocity model (described further later in this section). More typically, repeatability-scaling factors are estimated relative to a constant velocity model. The time series of daily coordinates relative to TVST, with 95% error bars, are shown in Fig. 2, and scaling factors for the formal errors are given in Table 1. The scaling factors given here are a factor of one to two smaller than would result using a constant velocity model, but are much smaller than have been reported in other studies (typically of order 10–15). This is largely because the formal error was estimated differently. However these error estimates are more rigorous than would obtain from the standard approach.

Small but significant motions were detected during

the first year of measurement: Relative coordinates changed by nearly 30 mm in the horizontal and 50 mm in the vertical for sites on Volcano Island, where baselines are very short (2.7 km to PINT; 5.8 km to KAYT). Coordinates for the longer (~65 km) baselines to Manila also changed by up to ~30 mm in the horizontal, but totaled as much as 120 mm in the vertical. The vertical varies more on the longer baselines in part because atmospheric bias errors in differential GPS primarily influence the vertical coordinate and increase with scale. Vertical motions due to groundwater withdrawal in Manila may contribute also. Regional-scale GPS campaign measurements document more than a meter of subsidence at some metro Manila sites between 1996 and 1998 (Thibault et al., 1999). Terrestrial surveys and mapping of surface ground cracks in early 1998 indicated that groundwater extraction was responsible for the subsidence.

Velocities of the sites are estimated from daily coordinates using a least squares regression with data kernel matrix weighted by: (1) the inverse formal variance of the daily coordinate solutions; and (2) a windowing function designed to emphasize motion at the center of the time window. Motions at Taal are small relative to coordinate error, so we use a 60-day triangular window in which the coordinate of the central day is given full weight, tapering to zero weighting at 30 days before and after. The length and shape of the window determine the tradeoff between resolution and variance of the velocity estimate (e.g. Menke, 1984), and ideally one would like to use the shortest window (highest resolution) that nevertheless provides high signal-to-noise ratio (low variance). We tested window lengths of 30 and 45 days, and window shapes including a box function and asymmetrical triangle or “ramp” function. Shorter windows provide velocity estimates with more high-frequency content, but also have lower mean *t*-test significance. A box function has lower resolution than a triangle function, and asymmetry introduces phase errors into the velocity variation (i.e. changes in velocity behavior are shifted in time from their actual locus). Hence we settled on the 60-day triangular window as an optimal tradeoff for the data we had. If signals were larger, one could use a shorter window and still yield velocities that are significant at high confidence.

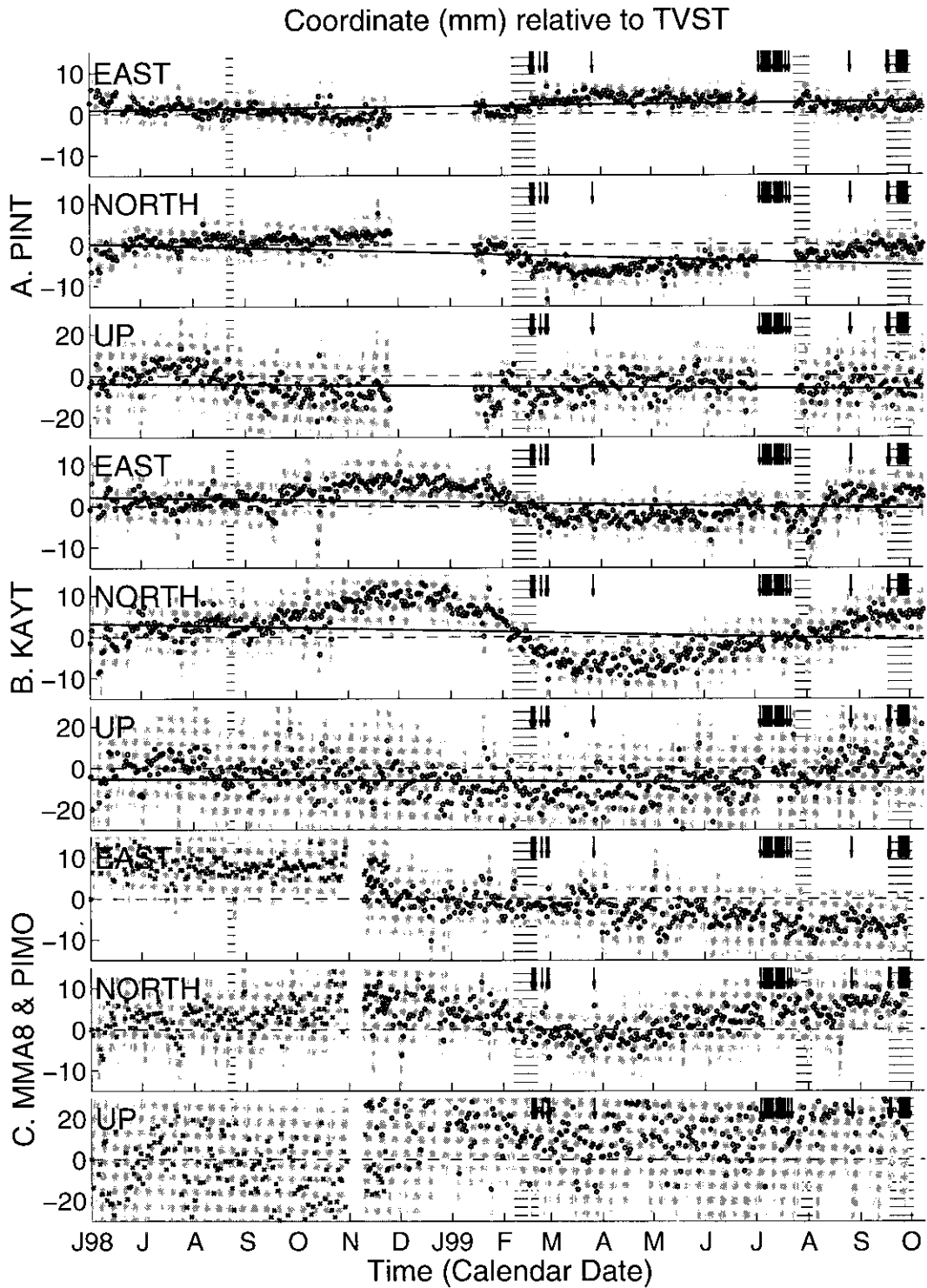


Table 1
Repeatability scale factors for formal errors

Baseline	North	East	Up
TVST-PINT	1.56829	1.95042	1.50962
TVST-KAYT	2.46790	2.85648	2.08290
TVST-MMA8	2.94261	3.71559	3.48761
TVST-PIMO	3.62822	3.94488	3.98844

The time series of velocity and scaled 95% error is given in Fig. 3. One will note that, near the endpoints of the time series, velocity variations are phase-shifted and have larger error because the regression window is truncated and asymmetric. However, velocities of the Taal sites exhibit temporal variability that is significant at very high confidence. Relative velocities were particularly high in early 1999, exceeding 150 mm yr⁻¹ in the horizontal on the KAYT-TVST baseline.

5. Volcanic source modeling

Relative velocities at the three stations were parameterized by a simple point source deformation model based on that of Mogi (1958). The model is commonly used to describe radial and vertical surface displacement due to pressure change in a spherical inclusion in an elastic half-space. We express the model in terms of our observables (i.e. 3-component GPS station velocity relative to the base station TVST) as:

$$V_i^j = K \frac{X_i^j - X_i^0}{[(X_1^j - X_1^0)^2 + (X_2^j - X_2^0)^2 + (X_3^j - X_3^0)^2]^{\frac{3}{2}}} - \nu_i^{\text{TVST}}. \quad (1)$$

Here, V_i^j is the relative velocity of the j th station in the i direction; X_i^j is position of the j th station; X_i^0 is position of the deformation point-source; $\bar{\nu}^{\text{TVST}}$ is true velocity of TVST in the reference frame of the deformation point-source; and K is a magnitude term combining time rate of change of volume \dot{V} and pres-

sure P of the spherical source with the shear rigidity μ of the elastic halfspace:

$$K = \frac{9}{16\mu\pi} \frac{\partial}{\partial t}(\dot{V}P). \quad (2)$$

A priori unknown model parameters in Eq. (1) include the source magnitude K , source position \bar{X}^0 , and TVST reference velocity $\bar{\nu}^{\text{TVST}}$ relative to the source. Given three components of relative velocity at all three stations (including $\bar{\nu}^{\text{TVST}} = \vec{0}$), we have a marginally overdetermined nonlinear system of 9 equations in 7 unknowns. We solve this system by combining a nonlinear, least-squares gradient search algorithm (e.g. Menke, 1984) with a grid search over plausible starting models. The gradient search converges to a solution using the Jacobian gradient matrix:

$$\bar{G} = \frac{\partial \bar{\mathcal{Y}}(\bar{m})}{\partial \bar{m}}, \quad (3)$$

for the model equation vector $\bar{\mathcal{Y}}$ (Eq. (1)) and unknown parameter vector \bar{m} . Model parameters are iteratively updated from the starting model \bar{m}_0 , with the linearizing correction:

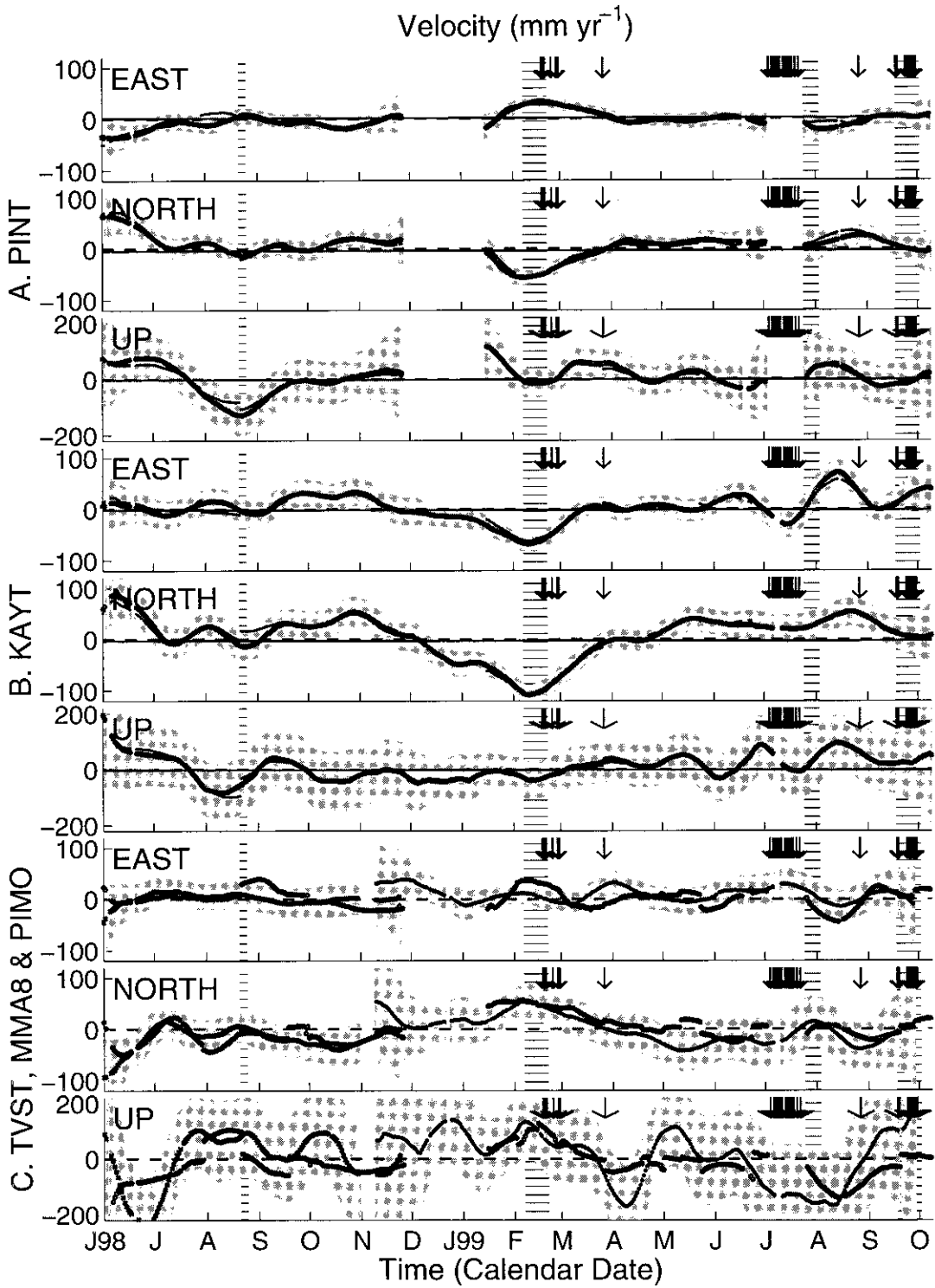
$$\Delta \bar{m}_{k+1} = [\bar{G}^T(\bar{m}_k)\bar{G}(\bar{m}_k)]^{-1}\bar{G}^T(\bar{m}_k)[\bar{d} - \bar{\mathcal{Y}}(\bar{m}_k)], \quad (4)$$

in which the data vector \bar{d} contains the observed velocities (\bar{V}^j). The grid search component of the inversion utilizes 648 starting models \bar{m}_0 , corresponding to inflationary and deflationary point sources positioned on a 1-km grid within a $5 \times 5 \times 6 \text{ km}^3$ volume centered beneath Taal's main crater. The resulting 648 estimates of model parameters tend to cluster in as many as 7 different local minima in the solution error space; we retain the solution with the smallest L_2 misfit error norm as the optimal model solution.

6. Model limitations

Time series of the best-fit source location \bar{X}^0 and source magnitude K are shown in Fig. 4. These model parameters generally vary smoothly in time, as would

Fig. 2. Time series of site coordinate change (in mm) relative to TVST. Gray bars are 95% formal error scaled to repeatability, horizontal bar pattern indicates periods of anomalous hydrothermal activity, vertical arrows denote >5 local high-frequency earthquakes per day. Solid black line is the best-fit secular velocity. Note the scale for the vertical coordinate is twice that for horizontal. (a) PINT; (b) KAYT; (c) Manila sites (\times = MMA8; \circ = PIMO).



be expected given the smooth variation of site velocities derived from 60-day windows. However, there are occasional abrupt changes in the deformation source parameters that might seem inconsistent with velocity smoothness. Mathematically, these discontinuities occur because the global minimum in the inversion error space occasionally shifts from one (smoothly varying) local minimum to another. Physically, this reflects: (1) inadequacies of the model; and (2) small signals relative to the noise in coordinate estimates. Inadequacies of the model include the assumptions of constant velocity for the 60-day estimation periods and of a single point source of deformation. In fact, velocities are highly variable in this dynamic environment, and there are probably many different deformation loci with more complicated moments than the scalar K assumed here, but the three-station network on Taal is not sufficient to constrain a more complex model with additional parameters. Noise in relative coordinate estimates is dominated by multipath and unmodeled atmospheric propagation effects, and is sufficiently large that the coordinate deviations are nonzero at 95% scaled confidence only about 25% of the time for the horizontal coordinates. Vertical coordinates exceed 95% confidence less than 6% of the time, i.e. hardly more than would be expected if there were no vertical motions at all.

The solution signal-to-misfit ratio $S = \|\vec{d}\|/\|\vec{d} - \vec{\mathfrak{F}}(\vec{m})\|$, in which $\|\cdot\|$ denotes the L_2 norm, is a useful measure of model significance because S will only be large when velocities are: (1) large relative to errors; and (2) consistent with a single scalar point source. The ratio S for model solutions in Fig. 4 ranges from 10 to 250, and is reflected in the scaling of symbols. The source location varies substantially over the period of observation, but deformation sources with large S (notably the deflation sequence during October–November of 1998 and inflation during February–March of 1999) are generally at depths of 2 to 5 km and within 2 km horizontally of Taal's main crater. Sources with small $S \lesssim 50$ are not significant at high confidence.

The deformation inversion scheme presented here differs substantially from most previous methodologies in that the reference frame of the network relative to the deformation source is included as a model parameter to be estimated. Reference frame velocity \vec{v}^{TVST} is shown in Fig. 3c along with velocities from the best-fitting model (superimposed black dots). Also shown in Fig. 3c are the velocities (with 95% error) of TVST relative to PIMO and MMA8, continuous sites in Manila for which velocities were estimated but not included in the inversion for deformation parameters. Defining a reference frame for the network relative to the deformation source is a necessary step in modeling of geodetic displacements. For GPS network data, this is most commonly done by fixing a reference site outside the area of influence of the deformation source, but we chose not to do this primarily because no place in the rapidly-deforming Philippine islands can be considered “stable” relative to Taal (e.g. Thibault, 1999). Solving for the reference frame also has potential drawbacks, however, because adding parameters to a nonlinear inversion can increase the nonuniqueness of the solution space. To test this we calculated the mean parameter correlation matrix \bar{R} for all solutions and found that, while most parameters have negligible cross-correlation, the vertical reference velocity v_U^{TVST} and source magnitude K have a very high correlation coefficient of ~ 0.9 . This indicates that the inversion has difficulty distinguishing a small source with a small vertical reference frame velocity from a large source with large v_U^{TVST} . The ambiguity stems from the placement of instruments approximately equidistant from the surface projection of main-crater deformation sources; in fact it can be shown that, for three perfectly equidistant stations, the source depth and reference velocity are mathematically indistinguishable. A better distribution of measurements (e.g. putting a station in the main crater) would help to resolve this ambiguity.

Nevertheless, the inverted reference velocity (including v_U^{TVST}) is strongly correlative with velocities of TVST relative to Manila sites, despite their independent estimation and the ambiguity of the

Fig. 3. Time series of velocity (in mm yr^{-1}). 95% error, hydrothermal activity and earthquakes are depicted as in Fig. 2. Dark grey circles for (a) PINT and (b) KAYT are observed velocity relative to TVST; small black dots are velocity of the best-fit point-source deformation model for that day. Dark grey circles in (c) are the inverted reference velocity of TVST relative to the deformation point source; black symbols are observed velocity of TVST relative to Manila sites (\times = MMA8; $+$ = PIMO) with corresponding 95% error.

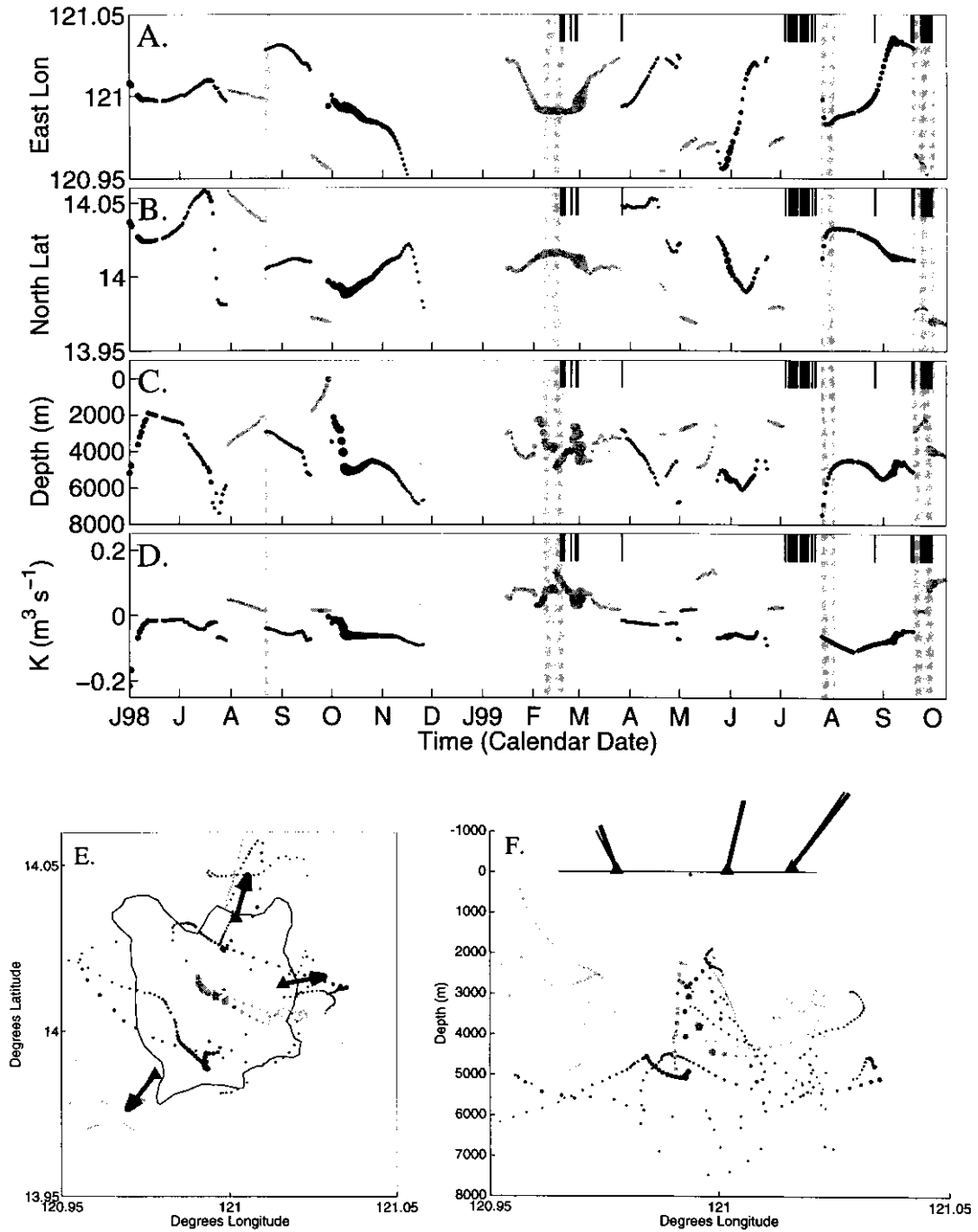


Fig. 4. Deformation model source parameters. (a)–(d) Time series of best-fit source location and magnitude term K . Black dots are deflationary sources; gray dots are inflationary; dot size is scaled by signal-to-misfit-ratio S . Earthquakes and hydrothermal events are depicted as in previous figures. (e) Source locations in map view. Arrows depict observed plus reference velocity (gray) and best-fit model velocity (thin black) for inflationary source of March 1, 1999, denoted by star. (f) Source locations in cross-section, looking north.

inverse method. There are some discrepancies, but disagreement does not necessarily indicate a faulty estimate of \bar{p}^{TVST} because the Manila sites are influenced by other (nonvolcanic) deformation sources such as groundwater subsidence and tectonic strain (Thibault, 1999), as well as larger errors in estimation of non-common-mode atmospheric delay. During the course of investigation we ran test inversions in which the Manila sites were incorporated into the data vector. The resulting deformation sources were generally in good agreement with those of Fig. 4 during periods when S is large, but at other times, inclusion of the Manila sites produced estimates of \bar{X}^0 well outside Taal's caldera region. Consequently, our preferred solution depicted in Fig. 4 solves for the reference frame velocity without incorporating Manila GPS data. Manila data are used only as an independent, a posteriori test of \bar{p}^{TVST} .

7. Discussion and conclusions

The dual-frequency GPS network installed on Taal in 1998 is capable of detecting fairly small motions in quasi-real time using standard geodetic processing. Moreover, the three stations on Volcano Island are sufficient to permit inversion for parameters of a simple point-source deformation model. However, with only three stations and motions near the noise level, the data are not sufficient to constrain more sophisticated models that might provide greater insight into processes of deformation. Deformation constraint could be improved substantially with the additional short-period sensitivity provided by tiltmeter or strainmeter data. One tiltmeter was in operation on Taal during at least part of the period covered by this analysis, and it would be relatively simple to include a description of tilt rate in the set of linear equations used to invert for deformation point sources. However, the tilt data were not available to us at the time of this study.

Despite the small signal-to-noise-ratio of the data used in this analysis, some information about deformation processes on Taal can be gleaned from comparison to other physical phenomena. The first sixteen months of continuous GPS measurement has been distinguished by unusual hydrothermal activity in Taal's main crater, including three spectacular

geyser sequences that prompted PHIVOLCS to issue low-level alerts and briefly close the island to tourism. The first of these events produced sustained fountaining to heights of 4–6 m and a 15-m-high mud splatter cone in February 1999, and it occurred right at the peak of the most significant strain event in the time series (Fig. 3). In all three sequences, the onset of geysering is accompanied by a rapid deceleration of southwestward motion of KAYT relative to TVST (other baselines are incomplete during later events). During February 1999 the deformation point source is estimated at depths of 2–5 km and the map-projected location is within a few hundred meters of the geyser activity. Assuming a residual magma body at a depth of ≥ 5 km beneath Taal's main crater, vigorous groundwater circulation would be expected in this volume and would be consistent with observed high seismic attenuation at shallow depths beneath Volcano Island (Nishigami et al., 1994) if that attenuation corresponds to hydrothermal alteration.

Dark gray dots in Fig. 4 indicate a deflationary source while light gray dots denote inflation. Deformation behavior flickers between inflationary and deflationary on time scales consistent with gradual pressurization and then sudden expulsion of hydrothermal fluids (with the latter expressed as surface geysering). The source magnitude term K (Fig. 4a) is typically about $\pm 0.05 \text{ m}^3 \text{ s}^{-1}$. K reflects rate of change of P and volumetric changes as a consequence of poroelastic effects in addition to the physical volume of the fluid itself, and so the volume of fluid flux cannot be estimated directly. K does have a physical significance relating to volume though; integration of Eq. (1) yields a net or "global" volumetric rate of change of $2\pi K \text{ m}^3 \text{ s}^{-1}$. Large-scale volumetric change rates of order $0.3 \text{ m}^3 \text{ s}^{-1}$ ($= 3 \times 10^{-5} \text{ km}^3 \text{ day}^{-1}$) are not unreasonable for hydrothermal flux.

Seismicity at Taal volcano also correlates with the velocity fluctuations and hydrothermal activity. Days on which more than five local earthquakes were recorded on Taal are denoted by arrows on the time series plots (Figs. 2–4), and virtually all seismicity clustering occurs in association with a hydrothermal event and a velocity peak on the TVST-KAYT baseline. Correlation of the seismicity and velocity is not surprising, as both are fundamentally expressions of strain. The seismicity trails the change in deformation behavior by several weeks to months, a phenomenon

previously noted in other studies of volcano deformation (e.g. Langbein et al., 1993; Dvorak and Dzurisen, 1997). This can be attributed to the time required for elastic strain to accumulate leading up to a critical state of failure in a dynamic environment.

The correlation of strain and seismicity to hydrothermal activity implies that deformation at Taal may be predominantly a poroelastic response to hydrothermal fluid migration. The relationship of the hydrothermal activity at Taal to magmatic processes — and hence, the implications of the 1999 phenomena for volcanic hazard analysis — is less clear. The dramatic hydrothermal events indicate some change in the system, but without more ancillary information, we are unable to distinguish a benign change in plumbing system or meteoric supply from a more ominous shift in volatile exsolution or a mobilization of meteoric water by magma migration. However, there is little in the literature to suggest that an increase in hydrothermal flux and associated seismicity can be construed as a reliable volcanic precursor. Many (if not most) large caldera-forming volcanoes are characterized by dynamic hydrothermal systems: much of the deformation and seismic swarm activity at Yellowstone, Long Valley, and Taupo appears to be expressing hydrothermal circulatory unrest (e.g. De Natale et al., 1991; Bibby et al., 1995; Wicks et al., 1998; Henderson et al., 1999), although a strong case can be made for a magmatic component at Long Valley (Battaglia et al., 1999).

Although deformation observed on Taal thus far appears to result from hydrothermal fluid migration, we continue to monitor for indications of anomalous motion that might be more directly attributable to magmatic processes. During June and July of 1999, we significantly augmented the GPS network with 12 single-frequency GPS stations: an additional 7 on Volcano Island, and 5 on the caldera rim (Bartel et al., 1999). As of this writing, the processing algorithms for analysis of these data are still in development, but we expect that our capacity to observe and interpret the processes responsible for deformation on Taal will be greatly enhanced in the near future.

Acknowledgements

This project would not have been possible without

the efforts of our many collaborators at PHIVOLCS, UNAVCO and Indiana University. We thank Raymundo Punongbayan and Ernesto Corpuz of the Philippine Institute of Volcanology and Seismology (PHIVOLCS) for generous organizational and maintenance support. Oivind Ruud, Cathy Thibault, Karl Feaux, Natalie Anderson, Agnes Aguilar, Ireneo Herald, Elmer Gabinete, Manuel Sexon and other members of the PHIVOLCS volcano monitoring team made generous contributions of their time and energy at various stages of the instrumentation and data routing. Beth Bartel's barrage of questions and legwork in compiling ancillary data helped us to greatly clarify significance of the model behavior. The paper was improved by suggestions of Susan Owen and an anonymous reviewer. This research was funded by NSF grants EAR-9727300 and EAR-9726024.

References

- Aoki, Y., Segall, P., Kato, T., Cervelli, P., Shimada, S., 1999. Imaging magma transport during the seismic swarm off the Izu Peninsula, Japan. *Science* 286, 927–930.
- Banks, N.G., Tilling, R.I., Harlow, D.H., Ewart, J.W., 1989. (Volcano monitoring and short-term forecasts). In: Tilling, R.I. (Ed.), *Volcanic Hazards*. Am. Geophys. Union, Washington, DC, pp. 51–80.
- Bartel, B.A., Hamburger, M.W., Lowry, A.R., Meertens, C., Reeder, S., Thibault, C.A., Ramos, E.G., Corpuz, E., Gabinete, E., Sexon, M., Aguilar, A.R., 1999. GPS measurement of volcanic deformation at Taal volcano, Philippines [abstract]. *EOS, Trans. Am. Geophys. Union*, 80 (46): F272.
- Battaglia, M., Roberts, C., Segall, P., 1999. Magma intrusion beneath Long Valley caldera confirmed by temporal changes in gravity. *Science* 285, 2119–2122.
- Besana, G.M., Shibutani, T., Hirano, N., Ando, M., Bautista, B., Narag, I., Punongbayan, R.S., 1995. The shear wave velocity structure of the crust and uppermost mantle beneath Tagaytay, Philippines, inferred from receiver function analysis. *Geophys. Res. Lett.* 22, 3143–3146.
- Beutler, G., Kouba, J., Springer, T., 1995. Combining the orbits of the IGS Analysis Centers. *Bull. Geodesique* 69, 200–222.
- Bibby, H.M., Caldwell, T.G., Davey, F.J., Webb, T.H., 1995. Geophysical evidence on the structure of the Taupo volcanic zone and its hydrothermal circulation. *J. Volcanol. Geotherm. Res.* 68, 29–58.
- De Natale, G., Pingue, F., Allard, P., Zollo, A., 1991. Geophysical and geochemical modelling of the 1982–1984 unrest phenomena at Campi Flegrei Caldera (southern Italy). *J. Volcanol. Geotherm. Res.* 48, 199–222.
- Dixon, T., Mao, A., Bursik, M., Heflin, M., Langbein, J., Stein, R., Webb, F., 1997. Continuous monitoring of surface deformation

- at Long Valley Caldera California with GPS. *J. Geophys. Res.* 102, 12,017–12,034.
- Dvorak, J.J., Dzurisen, D., 1997. Volcano Geodesy: The search for magma reservoirs and the formation of eruptive vents. *Rev. Geophys.* 35, 343–384.
- Hamburger, M.W., Cardwell, R.K., Isacks, B.L., 1983. Seismotectonics of the northern Philippine island arc. In: Hayes, D.E. (Ed.), *The Tectonic and Geologic Evolution of Southeast Asian Seas and Islands, Part 2*. AGU Geophys. Monogr. 27, pp. 1–22.
- Hamburger, M.W., Tomida, M., Thibault, C., Lowry, A.R., Ramos, E.G., Aguilar, A., Isada, M., Sexon, M., Banganan, E., Puertellano, J., Punongbayan, R.S., Feir, R., 1998. GPS and Seismotectonic Constraints on Crustal Deformation in the Northern Philippine Island Arc [abstract]. *EOS, Trans. Am. Geophys. Un.*, 79 (45): F202.
- Henderson, J.R., Barton, D.J., Foulger, G.R., 1999. Fractal clustering of induced seismicity in The Geysers geothermal area, California. *Geophys. J. Int.* 139, 317–324.
- Jousset, P., Okada, H., 1999. Post-eruptive volcanic dome evolution as revealed by deformation and microgravity observations at Usu volcano (Hokkaido, Japan). *J. Volcanol. Geotherm. Res.* 89, 255–273.
- Kato, T., Kotake, Y., Nakao, S., Beavan, J., Hirahara, K., Okada, M., Hoshihara, M., Kamigaichi, O., Feir, R.B., Park, P.H., Gerasimenko, M.D., Kasahra, M., 1998. Initial results from WING, the continuous GPS network in the western Pacific area. *Geophys. Res. Lett.* 25, 369–372.
- Knittel, U., Oles, D., 1995. Basaltic volcanism associated with extensional tectonics in the Taiwan-Luzon island arc: Evidence for non-depleted sources and subduction zone enrichment. In: Smellie, J.L. (Ed.), *Volcanism Associated with Extension at Consuming Plate Margins*. *Geol. Soc. London, Spec. Publ.* 81, 77–93.
- Langbein, J., Hill, D.P., Parker, T.N., Wilkinson, S.K., 1993. An episode of reinflation of the Long Valley caldera, eastern California: 1989–1991. *J. Geophys. Res.* 98, 15,851–15,870.
- Listanco, E., 1994. Space-time patterns in the geologic and magmatic evolution of calderas: a case study at Taal volcano, Philippines. PhD thesis, Tokyo University, Tokyo, Japan.
- Mattioli, G.S., Dixon, T.H., Fredric, F., Howell, E.S., Jansma, P.E., Smith, A.L., 1998. GPS measurement of surface deformation around Soufriere Hills volcano, Montserrat from October 1995 to July 1996. *Geophys. Res. Lett.* 25, 3417–3420.
- Menke, W., 1984. *Geophysical Data Analysis: Discrete Inverse Theory*. Academic Press, Orlando, FL.
- Miller, D.S., Smith, R.B., 1999. P and S velocity structure of the Yellowstone volcanic field from local earthquake and controlled source tomography. *J. Geophys. Res.* 104, 15,105–15,121.
- Mogi, K., 1958. Relation between eruptions of various volcanoes and the deformations of the ground surfaces around them. *Bull. Earthq. Res. Inst.* 36, 99–134.
- Moore, J.G., Nakamura, K., Alcaraz, A., 1966. The eruption of Taal volcano. *Science* 151, 955–960.
- Nishigami, K., Shibutani, T., Ohkura, T., Hirata, M., Horikawa, H., Shimizu, K., Matsuo, S., Nakao, S., Ando, M., Bautista, B.C., Bautista, L.P., Barcelona, E.S., Valerio, R., Lanuza, A.G., Chu, A.V., Villegas, J.J., Rasdas, A.R., Mangao, E.A., Gabinete, E., Punongbayan, B.J.T., Punongbayan, R.S., 1994. Shallow crustal structure beneath Taal volcano, Philippines, revealed by the Seismic Explosion Survey. *Bull. Disas. Prev. Res. Ins.*, Kyoto Univ. 44, 123–138.
- Omori, F., 1913. The Usu-san eruption and the earthquake and elevation phenomena II. *Bull. Imp. Earthq. Invest. Comm.* 5, 101–137.
- Owen, S., Segall, P., Freymueller, J., Miklius, A., Denlinger, R., Arnadottir, T., Sako, M., Burgmann, R., 1995. Rapid deformation of the south flank of Kilauea volcano, Hawaii. *Science* 267, 1328–1332.
- Owen, S., Segall, P., Lisowski, M., Miklius, A., Murray, M., Bevis, M., Foster, J., 2000. January 30 eruptive event on Kilauea volcano, Hawaii, as monitored by continuous GPS. *Geophys. Res. Lett.* (in press).
- Pingue, F., Troise, C., De Luca, G., Grassi, V., Scarpa, R., 1998. Geodetic monitoring of Mt. Vesuvius volcano, Italy, based on and GPS surveys, EDM. *J. Volcanol. Geotherm. Res.* 82, 151–160.
- Ramos, E.G., Punongbayan, R., Laguerta, E., Melosantos, A., Corpus, E., Vandemeulebrouck, J., Hamburger, M.W., 1997. Crustal deformation and seismic monitoring of volcanic activity at Pinatubo and Taal volcanoes, Philippines [abstract]. *Seismol. Res. Lett.*, 68: 327.
- Rothacher, M., Mervart, L. (Eds.), 1996. *Bernese GPS Software Version 4.0*. Astronomical Institute University of Berne, Berne, Switzerland.
- Silver, P.G., Bock, Y., Agnew, D., Henyey, T., Linde, A.T., McEvelly, T.V., Minster, J.B., Romanowicz, B., Sacks, I.S., Smith, R.B., Solomon, S.C., Stein, S.A., plate, A., 1999. boundary observatory. *IRIS Newsllett.* 16, 3–9.
- Taal Volcano Profile, 1995. Philippine Institute of Volcanology and Seismology report, 89 pp.
- Thibault, C.A., 1999. GPS measurement of crustal deformation in the northern Philippine island arc. Thesis, MS, Indiana University, 126 pp.
- Torres, R.C., Self, S., Punongbayan, R.S., 1995. Attention focuses on Taal: Decade volcano of the Philippines. *EOS, Trans. Am. Geophys. Union* 76, 241–247.
- Wicks, C., Thatcher, W., Dzurisen, D., 1998. Migration of fluids beneath Yellowstone caldera inferred from satellite radar interferometry. *Science* 282, 458–462.